MECHANICAL SIMULATION OF MULTICELLULAR STRUCTURES WITH THE MATERIAL POINT METHOD

James E. Guilkey[1], Yuan Zhang[2], James B. Hoying[3], Jeffrey A. Weiss[4]

1. ABSTRACT

The objective of this research was to develop and test a procedure for modeling the specimen-specific mechanical response of multicellular constructs to globally applied strains/stresses using the Material Point Method (MPM). Volumetric confocal image data of vascularized collagen constructs were used to generate particle distributions. Refinement and sensitivity studies were performed. A variant of the standard MPM algorithm, in which the background grid is not reset between computational cycles, was investigated. Results demonstrated that geometric representations could be generated easily from confocal image data. Despite the globally homogeneous applied strain, stress distribution in the vascular constructs was highly inhomogeneous. The modified MPM algorithm eliminated a common MPM artifact that results from particles crossing grid boundaries. This research demonstrates the feasibility of using meshless methods for specimen-specific analysis of complex multicellular constructs, enabling the study of the relationship between local cellular stresses and strains and cellular catabolic / anabolic responses to mechanical conditioning.

2. INTRODUCTION

Cells exhibit a wide range of responses to mechanical conditioning, including modification of the extracellular matrix (ECM) and alterations in cell adhesion. Thus, the effects of globally applied mechanical loads on local cell stresses and strains are an important topic in mechanobiology. Globally applied mechanical loading can result in highly inhomogeneous stress and strain fields around cells. Explicit microscale geometric and material representations are needed to calculate the local stress state, but standard numerical analysis techniques such as the finite element (FE) method are difficult to apply because of the highly complex geometry.

Previous efforts to model cells and cellular constructs have primarily used the FE method for spatial discretization. Applications include the study of leukocyte deformation [1], cell-tissue interactions [2], intracellular/extracellular fluid flow [3], chondrocyte interaction with the pericellular matrix [4] and micropipette aspiration [5,6]. The difficulty with application of the FE method to multicellular constructs is that a large specimen-specific model is often required to represent a significant portion of the overall domain of interest. The large, complex geometry of cellular constructs

[1] Research Assistant Professor, Department of Mechanical Engineering, University of Utah, 50 S Central Campus Dr. Rm 2110, Salt Lake City, UT, 84112, USA
[2] Ph.D. Student, Department of Bioengineering, University of Utah
[3] Associate Professor, Biomedical Engineering Program, University of Arizona, Life Sciences North Room 362 1501 N. Campbell Ave, Tucson, Arizona 85724
[4] Corresponding author. Associate Professor, Department of Bioengineering, Faculty Member, Scientific Computing and Imaging Institute, University of Utah, 50 S. Central Campus Dr. Rm 2480, Salt Lake City, UT 84112 USA

makes this task extremely difficult with the FE method. Meshless methods are especially attractive for these problems.

Our laboratory is studying the mechanical interactions of microvessel fragments with a synthetic extracellular matrix in the context of an in vitro model of angiogenesis [7]. The focus of this study is to investigate the influence of mechanical loading of the vascularized collagen scaffolds. The physical scale of interest is at the level of the cellular construct. A meshless method, referred to as the Material Point Method (MPM), was chosen to model the complex geometry of microvessel fragments and surrounding matrix and thus determine the relationship between globally applied strains and local stresses and strains around sprouting capillaries. [8-10]. The objectives of this study were 1) to develop a method to analyze specimen-specific mechanics of vascularized constructs using MPM, 2) to perform a sensitivity study to clarify the effects of microvessels on the mechanical behavior of collagen gels and 3) to conduct a convergence study to demonstrate the effect of grid and particle resolution.

3. METHODS

3.1 Implicit Material Point Method

MPM is a variant of the particle in cell methods that represents materials of interest by a collection of particles (material points) instead of connected elements. A regular structured grid is used as computational scratchpad for integration and solution of the weak form of the equations of motion (Figure 1). Implicit time integration is desirable for the presently considered analyses because they can be classified as quasi-static or low-rate dynamic. A complete description of the implicit MPM formulation can be found in our previous publication [8] – an overview is presented below for completeness, assuming quasi-static conditions and elastic material behavior to simplify the presentation. Assuming that a converged solution is available at time t, the computational algorithm to obtain a solution at time $t+dt$ can be described by the following steps:

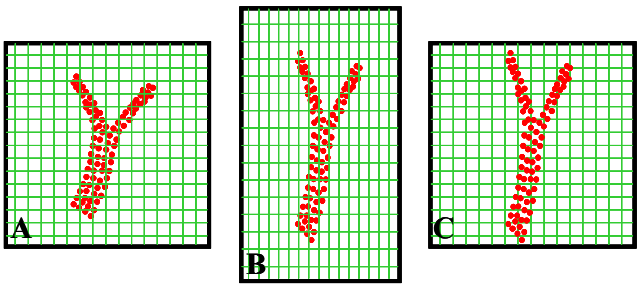

Figure 1: Schematic of a single computational step in MPM algorithm. A) Initial distribution of particles (red) and background computational grid (green). B) Stretching (vertical) and contraction (lateral) applied to particles. Computational grid convects with particles. C) Computational grid is reset and particles remain deformed/convected.

1) Interpolate the displacements $\boldsymbol{u}_p(t)$ and new external forces $\boldsymbol{Fext}_p(t+dt)$ to the computational grid to yield nodal values on the grid $\boldsymbol{u}_g(t)$ and $\boldsymbol{Fext}_g(t+dt)$, using the particle masses $m_p(t)$ for weighting. Grid nodes receive contributions from particles that are currently residing in grid elements that are constructed using that node, interpolated via the grid shape functions:

$$\boldsymbol{u}_g(t) = \frac{\sum_p \left(S_{gp} m_p(t) \boldsymbol{u}_p(t)\right)}{\sum_p \left(S_{gp} m_p(t)\right)}, \quad \boldsymbol{Fext}_g(t) = \sum_p S_{gp} \boldsymbol{Fext}_p(t). \tag{1}$$

2) Compute the deformation gradient $\boldsymbol{F}_p(t)$ at the current particle locations $\boldsymbol{x}_p(t)$

using $\boldsymbol{u}_g(t)$ from Equation (1):

$$\boldsymbol{F}_p(t) = \left(\boldsymbol{G}_p \boldsymbol{u}_g(t) + \boldsymbol{1}\right). \tag{2}$$

$\boldsymbol{G}_p$ is a matrix containing gradients of the shape functions evaluated at current particle coordinates $\boldsymbol{x}_p(t)$ and $\boldsymbol{1}$ is the identity tensor. The Cauchy stress $\boldsymbol{\sigma}_p\left(\boldsymbol{F}_p(t)\right)$ and spatial elasticity tensor $\boldsymbol{D}_p\left(\boldsymbol{F}_p(t)\right)$ are then calculated from the constitutive model.

3) Evaluate the internal force vector $\boldsymbol{Fint}_g(t)$ and tangent stiffness matrix $\boldsymbol{KK}_g(t)$:

$$\boldsymbol{Fint}_g(t) = \sum_e \int_{\Omega e} \boldsymbol{B}_L^T \boldsymbol{\sigma}_p dv\,, \tag{3}$$

$$\boldsymbol{KK}_g(t) = \boldsymbol{Kmat}_g(t) + \boldsymbol{Kgeo}_g(t)\,, \tag{4}$$

$$\boldsymbol{Kmat}_g(t) = \sum_e \int_{\Omega e} \boldsymbol{B}_L^T \boldsymbol{D}_p \boldsymbol{B}_L dv\,, \tag{5}$$

$$\boldsymbol{Kgeo}_g(t) = \sum_e \int_{\Omega e} \boldsymbol{B}_{NL}^T \boldsymbol{\sigma}_p \boldsymbol{B}_{NL} dv\,. \tag{6}$$

$\boldsymbol{B}_L$ and $\boldsymbol{B}_{NL}$ are the standard linear and nonlinear strain-displacement matrices encountered in a nonlinear finite element formulation [11] and Σ_e represents element assembly, processing contributions from grid nodes into the global arrays.

4) Solve the discrete equilibrium equations linearized about a configuration at time t iteratively for the incremental displacements $\boldsymbol{du}_g^k$ using Newton's method [11]:

$$\boldsymbol{KK}_g(t) \cdot \boldsymbol{du}_g = \boldsymbol{Fext}_g(t+dt) - \boldsymbol{Fint}_g(t). \tag{7}$$

The nodal displacements are accumulated each iteration by:

$$\Delta \boldsymbol{u}_g = \Delta \boldsymbol{u}_g + \boldsymbol{du}_g\,, \tag{8}$$

$$\boldsymbol{u}_g(t+dt) = \boldsymbol{u}_g(t) + \Delta \boldsymbol{u}_g\,. \tag{9}$$

where $\Delta \boldsymbol{u}_g$ is zeroed out at the beginning of each timestep. The values of $\boldsymbol{KK}_g(t)$ and $\boldsymbol{Fint}_g(t)$ are then updated appropriately. The optimal $\boldsymbol{du}_g$ minimizes the L^2 norm of the right-hand side of equation (7). The repeated solution of this linear system is performed using a conjugate gradient solver with a Jacobi preconditioner [12].

5) Save converged state ($\boldsymbol{F}_p(t+dt)$, $\boldsymbol{Fint}_g(t+dt)$ and $\boldsymbol{KK}_g(t+dt)$), update kinematics:

$$\boldsymbol{u}_p(t+dt) = \boldsymbol{u}_p(t) + \sum_g S_{gp} \Delta \boldsymbol{u}_g\,, \tag{10}$$

$$\boldsymbol{x}_p(t+dt) = \boldsymbol{x}_p(t) + \sum_g S_{gp} \Delta \boldsymbol{u}_g\,. \tag{11}$$

6) Reset the grid to its original (typically Cartesian) configuration.
7) Continue to next time step.

This algorithm can result in an artifact when particles cross grid boundaries [13], which can be especially troublesome for quasi-static simulations since there are no inertial forces. We investigated a modified algorithm in which the background grid geometry is not reset after each MPM computational cycle ("no reset") and compared its performance to the standard MPM procedure ("reset").

3.2 In vitro Model, Confocal Imaging and Particle Generation

This research is based around a three-dimensional in vitro model of angiogenesis, wherein microvessel fragments are isolated and cultured in a three-dimensional collagen gel [14]. Isolated vessel elements contain associated perivascular cells and spontaneously grow as patent tubes through the elaboration of numerous vessel sprouts.

These vessels continue to grow into a new vascular network that ultimately fills the gel space. Isolated vessel fragments include the full spectrum of vessel elements in the microvasculature, namely arterioles, capillaries and venules [7]. These microvessels retain the ability to form a functional vascular tree when implanted [15], supporting the notion that such cultured microvessels are healthy, normal and functional.

One vascularized gel cultured for 10 days was harvested and stained en bloc with an endothelial cell-specific lectin called GS-1, directly bound to fluorescein. A volumetric confocal image dataset (512(x) x 512(y) x 52(z), x-y dimensions 537.6 x 537.6 μm, section thickness 1.0 μm) was obtained with a Bio-Rad MRC-1024ES Confocal Laser Scanning Microscope fitted with a 40X objective (Figure 2, left panel). A bin thresholding algorithm was used to obtain a binary image. Microvessel volume fraction was calculated from the thresholded dataset. Finally, a collection of over 13 million material points was created by distributing material points in the image voxels (Figure 2, right panel). The calculation area is determined based on the needed spacing of particles and associated computational grid.

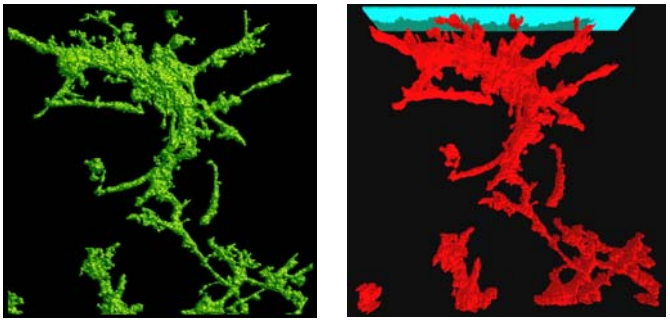

Figure 2: Left – volume rendering of original confocal microscopy data, showing a portion of a typical microvascular construct in collagen at Day 10 of culture. Right – initial distribution of material particles (collagen particles not shown for clarity). Direction of tensile loading is vertical.

3.3 Constitutive Model and Material Properties

The material properties of collagen gels are nonlinear and viscoelastic, while there are no data on material properties of microvessel fragments. As a first order approximation, an uncoupled compressible neo-Hookean hyperelastic constitutive model was used to represent the collagen and microvessels, with strain energy W [16]:

$$W = U(J) + \tilde{W}(\tilde{\boldsymbol{C}}) . \tag{12}$$

Here $\tilde{W}(\tilde{\boldsymbol{C}}) = \frac{\mu}{2}(I_1 - 3)$, $U(J) = \frac{k}{2}[\ln(J)]^2$, J is the volume ratio, μ is the shear modulus, k is the bulk modulus, and $\tilde{I}_1 = \mathrm{tr}(\tilde{\boldsymbol{C}})$ is the 1st invariant of the deviatoric right deformation tensor $\tilde{\boldsymbol{C}}$. The shear modulus of the collagen gel (μ = 520.8 Pa) was based on our experimental data [14]. To assess the effects of the microvessels on the material response of the vascularized scaffold, the microvessel particles were assumed to have twice shear modulus of the collagen. The bulk modulus for both the collagen and the microvessels was unknown and was thus arbitrarily chosen to yield a Possion's ratio of 0.4, resulting in slightly compressible behavior. Additional analyses were performed with all particles assigned the material properties of collagen for comparison.

3.4 Computational Analysis

To simulate extension of the vascular construct, the bottom of the domain was fixed and an extension was prescribed to the top to achieve 10% global strain. The fully three dimensional nonlinear problem was solved on 128 processors of a Xeon cluster using MPI. The computation required 2 hours of wall clock time. Results were processed to determine reaction force at the clamped end and spatial distribution of von Mises stress.

While the goals of this research will eventually require large numbers of 3D simulations, current efforts are focused on better understanding the effects of grid resolution and particle distribution on the quality of the simulation results. Specifically, a convergence study was performed to assess the effects of these factors on the resulting reaction force and von Mises stress distribution (Figure 3). These initial studies are being carried out in 2D using just 1 of the 52 slices that comprised the confocal data set.

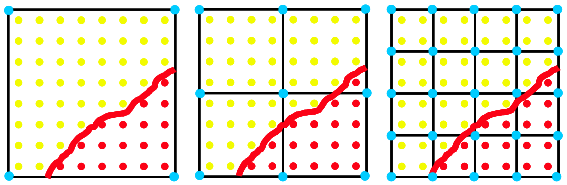

Figure 3: Schematic of particle and grid configurations investigated in the studies of grid and particle resolution. In all cases, the entire volume is 8.4 x 8.4 x 2.0 μm. Yellow points represent material points associated with the collagen, red points are associated with a blood vessel, aqua points are nodes in the computational grid and black lines denote the boundaries of grid cells.

4. RESULTS

The computed volume fraction of the microvessels was 19.4%. The stress distribution in the vascularized constructs was highly inhomogeneous (Figure 4), consistent with the hypothesis that local stress around cells and cellular constructs is inhomogeneous even under simple tensile loading. For the standard MPM algorithm, all particle/grid resolutions exhibited artifacts that were due to particles crossing grid boundaries (Figure 5, left panel). In contrast, when the background grid was not reset, the traction force on the top of the gels was nearly linear with applied strain, which is consistent with the nearly linear material behavior of the neo-Hookean constitutive model. There was a 7.4% difference in the traction force at 10% tensile strain between the cases of collagen only and collagen + microvessels for the most resolved case.

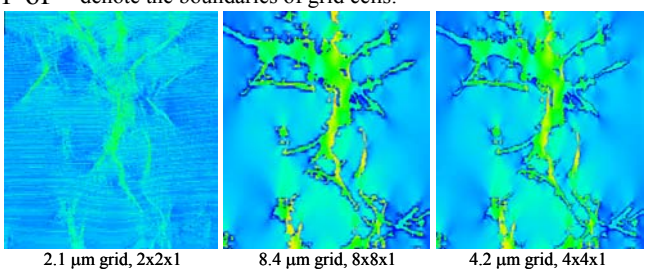

Figure 4: Effects of resetting the grid and particle/grid resolution on the spatial distribution of von Mises stress. Left panel – standard MPM algorithm resets the grid, resulting in significant artifacts in the stress field due to particles crossing grid boundaries. Middle and right panels –results for two different particle/grid resolutions without resetting the grid. Stress field artifact is eliminated, resulting stress field is highly inhomogeneous, and there are only minor differences between the two cases. Case represented by middle panel incurs significantly less computational expense.

5. DISCUSSION

This research demonstrates the feasibility of using MPM for computational modeling of the mechanics of multicellular constructs. Meshless methods have several significant advantages for the simulation of multicellular structures. First and foremost, 3D distributions of particles for computational modeling can

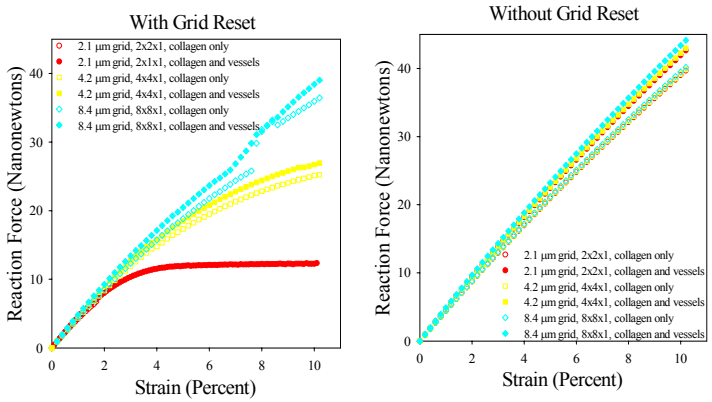

Figure 5: Effects of solution algorithm, grid/particle resolution and presence of vessels on clamp reaction force. Left - results for standard MPM algorithm (reset). Right - results for modified algorithm (no reset). Left graph shows significant errors in computed reaction force due to particles crossing cell boundaries. This problem is somewhat alleviated when the ratio of particles-per-cell to grid cell size is maximized. Right graph demonstrates that all three resolutions give acceptable results when the background grid is not reset.

be generated directly from confocal microscopy or other types of image datasets on a specimen-specific basis. Second, between-material contact is easily represented without specific representation of the material boundaries [17]. Finally, MPM avoids issues of element inversion and mesh entanglement during the simulations that can plague FE-based simulation techniques. A minor weakness with MPM is the additional computational costs associated with interpolations from the particles to the grid and back. Additional research is needed to develop optimal interpolation functions between the particles and the grid. Although our present focus is on modeling the interaction of cellular constructs with ECM, MPM and other meshless methods can be readily applied to simulate the mechanics of single cells, cell membranes, intracellular organelles and the cytoskeleton, using volumetric image data as a basis for model generation.

6. ACKNOWLEDGMENTS

Financial support from NIH #R01 HL077683, NIH #R01 HL67067, DOE #W-7405-ENG-48 and NSF-ITR #CTS0218574 is gratefully acknowledged.

7. REFERENCES

[1] Dong, C. and Skalak R., Leukocyte deformability: finite element modeling of large viscoelastic deformation, J Theor Biol, 1992, 158:173-93.

[2] Barocas, V. H. and Tranquillo R. T., A finite element solution for the anisotropic biphasic theory of tissue- equivalent mechanics: the effect of contact guidance on isometric cell traction measurement, J Biomech Eng, 1997, 119:261-8.

[3] Lei, X., Lawrence M. B. and Dong C., Influence of cell deformation on leukocyte rolling adhesion in shear flow, J Biomech Eng, 1999, 121:636-43.

[4] Wu, J. Z. and Herzog W., Finite element simulation of location- and time-dependent mechanical behavior of chondrocytes in unconfined compression tests, Ann Biomed Eng, 2000, 28:318-30.

[5] Drury, J. L. and Dembo M., Aspiration of human neutrophils: effects of shear thinning and cortical dissipation, Biophys J, 2001, 81:3166-77.

[6] Shao, J. Y., Finite element analysis of imposing femtonewton forces with micropipette aspiration, Ann Biomed Eng, 2002, 30:546-54.

[7] Hoying, J. B., Boswell C. A. and Williams S. K., Angiogenic potential of microvessel fragments established in three-dimensional collagen gels, In Vitro Cell Dev Biol, 1996, 32:402-419

[8] Guilkey, J. E. and Weiss J. A., Implicit time integration for the Material Point Method: Quantitative and algorithmic comparisons with the Finite Element Method., International Journal for Numerical Methods in Engineering, 2003, 57:1323-1338.

[9] Bardenhagen, S. G., Brackbill J. U. and Sulsky D., The material-point method for granular materials, Computer Methods in Applied Mechanics and Engineering, 2000, 187:529-541.

[10] Sulsky, D., Chen Z. and Schreyer H. L., A particle method for history dependent materials, Computer Methods in Applied Mechanics and Engineering, 1994, 118:179-196.

[11] Bathe, K.-J. Finite Element Procedures in Engineering Analysis. New Jersey 1982.

[12] Balay, S., Buschelman K., Gropp W. D., Kaushik D., Knepley M., McInnes L. C., F. S. B. and Zhang H. PETSc User's Manual. Rep. ANL-95/11 - Revision 2.1.3, Argonne National Laboratory,2002

[13] Zhou, S. The numerical prediction of material failure based on the material point method. PhD thesis. University of New Mexico 1998

[14] Krishnan, L., Weiss J. A., Wessman M. D. and Hoying J. B., Viscoelastic characterization of collagen gels for culture of tissues and cells, Tissue Engineering, 2004, 10:241-252

[15] Hoying, J. B., Shepherd B., Chen H. Y. S. and Williams S. K., Rapid perfusion of a prevascularized tissue construct following implantation, Laboratory Investigation, 2004, In Review.

[16] Simo, J. C. and Hughes T. J. R. Computational Inelasticity. New York 1998.

[17] Bardenhagen, S. G., Guilkey J. E., Roessig K. M., Brackbill J. U., Witzel W. M. and Foster J. C., An improved contact algorithm for the Material Point Method and application to stress propagation in granular material, Computer Modeling in Engineering and Sciences, 2001, 2:509-522.